

Orthoferrosilite: High-temperature crystal chemistry

SHIGEHO SUENO¹

Department of Earth and Space Sciences, State University of New York,
Stony Brook, New York 11794

MARYELLEN CAMERON

Board of Earth Sciences, University of California, Santa Cruz
Santa Cruz, California 95064

AND C. T. PREWITT

Department of Earth and Space Sciences, State University of New York,
Stony Brook, New York 11794

Abstract

The high-temperature crystal structure of orthoferrosilite (FeSiO_3 ; space group $Pbca$) has been examined using intensity data collected at 24°C, 400°C, 600°C, 800°C, 900°C, and 980°C. Structural changes between 24°C and 980°C were regular, and no transformations were observed. Mean Si-O bond lengths and tetrahedral volumes decrease slightly with increasing temperature, whereas mean Fe1-O and Fe2-O bonds show significant increases. Mean thermal expansion coefficients of the mean Fe1-O and Fe2-O distances in orthoferrosilite are larger than that observed for the Fe^{2+} -O bond in the $C2/c$ hedenbergite structure. Both the *A* and *B* tetrahedral chains in orthoferrosilite straighten with increasing temperature and, at 980°C, the *A* chain is almost completely extended. The change in the O3-O3-O3 angle is much larger than in $C2/c$ pyroxenes for comparable temperature intervals. A new notation describing the tetrahedral chain rotation (*N* or *P*) and the configuration around the *M2* site is introduced to aid in understanding differences among the various pyroxene structures.

Introduction

Although a natural occurrence of pure ferrosilite (FeSiO_3) has not been reported and all polymorphs of this composition are stable only at high pressure (Lindsley, 1965), this material is of considerable interest because it is one of the end-members of the pyroxene quadrilateral (MgSiO_3 - $\text{CaMgSi}_2\text{O}_6$ - $\text{CaFeSi}_2\text{O}_6$ - FeSiO_3). In a study on the stability of ferrosilite, Lindsley, MacGregor, and Davis (1964) reported the occurrence of three polymorphs. Subsequent structural investigation of these polymorphs (Burnham, 1966) revealed that one, ferrosilite III (space group $P\bar{1}$), has a pyroxenoid structure and that the other two, clinoferrosilite (space group $P2_1/c$) and orthoferrosilite (space group $Pbca$), have pyroxene structures.

Because the metal sites in ferrosilite are occupied only by Fe^{2+} , the high-temperature diffraction experiments on orthoferrosilite discussed in this paper provide valuable information on structural thermal expansion and atomic vibrations, especially when combined with similar data for other end-member pyroxenes (Cameron, Sueno, Prewitt, and Papike, 1973). In particular, this work represents: (1) the first high-temperature structural investigation of an end-member $Pbca$ orthopyroxene, and (2) the first thermal expansion data on a pyroxene whose *M2* site is completely occupied by iron.

Experimental

X-ray intensity data collection

Single crystals of orthoferrosilite, synthesized hydrothermally at 800°C and 20 kbar for 16 days, were kindly supplied by Dr. D. H. Lindsley. A single crystal, $0.08 \times 0.08 \times 0.08$ mm, was selected for X-ray

¹ Present address: Institut für Kristallographie und Mineralogie der Univ., 8 München 2, Theresienstr 41, West Germany.

diffraction intensity measurement. It was mounted parallel to the c axis on a silica glass fiber using a high-temperature ceramic cement, and sealed in an evacuated silica glass capillary to prevent oxidation of iron. The details of the heater and the cement were described by Brown, Sueno, and Prewitt (1973).

The X-ray diffraction intensities ($\sin \theta/\lambda = 0.061 \rightarrow 0.756$) were measured at several temperatures (24°C, 400°C, 600°C, 800°C, 900°C, and 980°C) on a PDP-15/35 computer-controlled Picker diffractometer in the ω - 2θ mode using $\text{MoK}\alpha$ radiation monochromatized with a graphite crystal. All the data were converted to structure factors by applying Lorentz and polarization corrections, but no absorption corrections were made. Just after the intensity data collection of each temperature, 20 independent 2θ values were measured for cell parameter determinations, and these data were used to refine the cell parameters in the PODEX-2 least-squares program written by Sleight. Final cell parameters are listed in Table 1.

Refinement

Full-matrix, least-square structure refinements for each temperature were carried out using the RFINE program written by L. Finger (Geophysical Laboratory) and atomic scattering factors for neutral atoms (Doyle and Turner, 1968). Starting atom coordinates and temperature factors for the 24°C structure refinement were taken from the room-temperature orthoferrosilite structure given by Burnham (1966). The starting atom coordinates for the high-temperature structure refinements were taken from those of the lower temperature structures.

All observations were weighted according to $w = 1/\sigma_F^2$ where σ_F is the standard error of the structure factor based on counting statistics (Prewitt and Sleight, 1968). All reflections which were indistinguishable from background or which had asymmetric backgrounds were rejected from the least-squares refinements. Table 2 lists the number of reflections collected at each temperature (excluding the standard reflection which was checked every 20 re-

flections), the number used for the final cycle of refinement, and the final weighted R factors.²

The results of the high-temperature structure refinements of orthoferrosilite are reported as follows: positional parameters and isotropic temperature factors, Table 3; interatomic distances in tetrahedral chains, Table 4; interatomic angles in tetrahedral chains, Table 5; Fe-O interatomic distances and O-O distances in Fe coordination polyhedra, Table 6; selected interatomic angles in Fe-coordination polyhedra, Table 7; and magnitude and orientation of thermal ellipsoids, Table 8.

Throughout this paper the term mean thermal expansion coefficient (MTEC) is used to describe the expansion of cell dimensions and interatomic distances with increasing temperature. The MTEC was calculated using the following equation:

$$\alpha_x = \frac{1}{X_{24}} \cdot \frac{X_T - X_{24}}{T - 24} \circ C^{-1}$$

where X_{24} and X_T are the values of a parameter at 24°C and at some higher temperature. See Cameron *et al* (1973) for further explanation.

Discussion

The *Pbca* orthopyroxene structure

A projection along a^* of part of the orthoferrosilite structure is shown in Figure 1. The $M1$ and $M2$ sites are occupied by Fe^{2+} , and at room temperature both are six-coordinated with the $M1$ coordination polyhedron being the smaller and more regular of the two. There are two symmetrically independent tetrahedral sites, each of which is confined to one chain. The two distinct chains are designated A and B , following the notation of Burnham (1966). The B chain is the more kinked of the two, and the tetrahedra comprising this are both larger and more distorted than those of the A chain. The tetrahedra of both chains are completely occupied by silicon.

There are six crystallographically nonequivalent oxygen atoms in the structure. $O1A$, $O2A$, $O1B$, and $O2B$ are nonbridging oxygens (each bonded only to one Si), and $O3A$ and $O3B$ are bridging oxygens (each bonded to two Si atoms). The nonbridging oxygens connect tetrahedral chains and $M1$ octahedral strips vertically along a^* and laterally along b

TABLE 1. Unit-Cell Parameters of Orthoferrosilite at Several Temperatures

	24°C	400°C	600°C	800°C	900°C	980°C
a (Å)	18.418(2)*	18.484(1)	18.527(1)	18.569(1)	18.596(1)	18.614(1)
b (Å)	9.078(1)	9.124(1)	9.145(1)	9.160(1)	9.168(5)	9.172(1)
c (Å)	5.2366(4)	5.2593(3)	5.2756(4)	5.2974(4)	5.3113(3)	5.3199(4)
v (Å ³)	875.6(1)	886.9(1)	893.9(1)	901.1(1)	905.5(1)	908.2(1)

* Errors in parentheses represent one standard deviation.

² To obtain observed structure factors and β_{ij} 's from the final cycle of each anisotropic refinement, order document AM-76-011 from the Business Office, Mineralogical Society of America, suite 1000 lower level, 1909 K Street, N.W., Washington, D.C. 20006. Please remit \$1.00 for the microfiche.

TABLE 3. Final Positional Parameters and Equivalent Isotropic Temperature Factors (Å) for Orthoferrosilite

Atom	Parameter	24°C	400°C	600°C	800°C	900°C	980°C
Fe1	x	0.37573(3)*	0.37554(4)	0.37517(5)	0.37499(6)	0.37492(6)	0.37467(7)
	y	0.65415(7)	0.65283(8)	0.65204(9)	0.65130(9)	0.6510(1)	0.6505(1)
	z	0.8746(1)	0.8823(2)	0.8869(2)	0.8926(2)	0.8968(2)	0.8992(2)
	B	0.46(1)	1.09(2)	1.42(2)	1.80(2)	1.98(2)	2.27(2)
Fe2	x	0.37766(4)	0.37724(5)	0.37714(6)	0.37666(7)	0.37641(8)	0.37637(8)
	y	0.48567(7)	0.48683(9)	0.4876(1)	0.4885(1)	0.4886(1)	0.4886(1)
	z	0.3667(1)	0.3748(2)	0.3805(2)	0.3879(2)	0.3926(2)	0.3964(3)
	B	0.62(1)	1.48(2)	2.01(2)	2.55(2)	2.83(3)	3.19(3)
SiA	x	0.27229(6)	0.27223(7)	0.27247(8)	0.27259(9)	0.27267(9)	0.2729(1)
	y	0.3387(1)	0.3384(2)	0.3376(2)	0.3369(2)	0.3371(2)	0.3374(3)
	z	0.0493(2)	0.0562(3)	0.0598(3)	0.0644(3)	0.0675(3)	0.0695(4)
	B	0.47(2)	0.86(2)	1.09(3)	1.33(3)	1.51(3)	1.64(4)
SiB	x	0.47310(6)	0.47356(7)	0.47411(8)	0.47462(9)	0.4752(1)	0.4755(1)
	y	0.33448(1)	0.3348(2)	0.3350(2)	0.3358(2)	0.3358(2)	0.3353(3)
	z	0.7891(2)	0.7862(3)	0.7827(3)	0.7783(3)	0.7742(3)	0.7725(4)
	B	0.42(2)	0.82(2)	1.09(3)	1.34(3)	1.47(3)	1.70(4)
O1A	x	0.1848(2)	0.1852(2)	0.1854(2)	0.1855(2)	0.1856(3)	0.1862(3)
	y	0.3396(3)	0.3386(4)	0.3393(5)	0.3390(5)	0.3386(6)	0.3394(7)
	z	0.0387(6)	0.0490(7)	0.0532(8)	0.0605(8)	0.0648(8)	0.0669(10)
	B	0.60(5)	1.18(6)	1.45(7)	1.77(8)	2.15(9)	2.26(10)
O2A	x	0.3118(2)	0.3113(2)	0.3112(3)	0.3115(3)	0.3115(3)	0.3120(3)
	y	0.4964(4)	0.4951(4)	0.4932(5)	0.4926(6)	0.4917(6)	0.4910(6)
	z	0.0582(6)	0.0695(7)	0.0756(8)	0.0832(9)	0.0856(10)	0.0921(11)
	B	0.68(5)	1.33(7)	1.92(8)	2.30(9)	2.54(10)	2.67(11)
O3A	x	0.3025(2)	0.3022(2)	0.3014(2)	0.3011(2)	0.3013(2)	0.3005(3)
	y	0.2363(4)	0.2406(5)	0.2434(5)	0.2450(6)	0.2470(7)	0.2491(7)
	z	0.8163(6)	0.8204(8)	0.8192(8)	0.8227(8)	0.8239(8)	0.8225(9)
	B	0.70(5)	1.44(7)	1.80(8)	2.45(10)	2.57(11)	2.87(13)
O1B	x	0.5610(2)	0.5613(2)	0.5613(2)	0.5617(2)	0.5622(2)	0.5623(3)
	y	0.3365(4)	0.3380(4)	0.3379(5)	0.3392(5)	0.3396(6)	0.3401(7)
	z	0.7868(6)	0.7838(7)	0.7812(8)	0.7771(9)	0.7731(9)	0.7727(10)
	B	0.71(5)	1.22(6)	1.72(7)	1.94(8)	2.20(9)	2.49(11)
O2B	x	0.4332(2)	0.4334(2)	0.4340(2)	0.4339(3)	0.4342(3)	0.4348(3)
	y	0.4806(3)	0.4806(4)	0.4825(5)	0.4832(6)	0.4846(6)	0.4847(7)
	z	0.6932(6)	0.6965(8)	0.7011(9)	0.7064(10)	0.7077(10)	0.7117(11)
	B	0.69(5)	1.39(7)	1.79(8)	2.24(10)	2.41(10)	3.13(13)
O3B	x	0.4476(2)	0.4481(2)	0.4487(2)	0.4488(3)	0.4500(3)	0.4493(3)
	y	0.2028(3)	0.2073(4)	0.2100(5)	0.2167(6)	0.2189(7)	0.2229(8)
	z	0.5865(6)	0.5782(7)	0.5719(8)	0.5604(9)	0.5521(9)	0.5455(10)
	B	0.60(5)	1.26(7)	1.76(8)	2.42(10)	2.71(11)	3.29(13)

* Errors in parentheses are one standard deviation.

TABLE 4. Interatomic Distances in Tetrahedral Chains in Orthoferrosilite at Several Temperatures

SiA	24°C	400°C	600°C	800°C	900°C	980°C	MTEC ($\times 10^{-5}$)
Si(A)-01A	1.613(3)*	1.608(4)	1.613(4)	1.617(5)	1.620(5)	1.615(5)	0.4358
02A	1.607(3)	1.603(4)	1.596(5)	1.602(5)	1.594(5)	1.590(6)	-0.9357
03A	1.652(3)	1.661(4)	1.646(4)	1.648(5)	1.653(5)	1.645(5)	-0.4536
03A'	1.633(3)	1.625(4)	1.625(4)	1.621(5)	1.624(5)	1.627(5)	-0.4792
Mean	1.626	1.624	1.620	1.622	1.623	1.619	-0.3495
SiB-01B	1.621(3)	1.622(4)	1.616(4)	1.618(5)	1.619(5)	1.616(5)	-0.2926
-02B	1.598(3)	1.595(4)	1.599(4)	1.594(5)	1.602(5)	1.599(6)	0.1358
-03B	1.666(3)	1.665(4)	1.663(5)	1.659(5)	1.662(5)	1.661(6)	-0.3682
-03B'	1.662(3)	1.651(4)	1.649(5)	1.642(5)	1.628(5)	1.622(6)	-2.3439
Mean	1.637	1.633	1.632	1.628	1.628	1.624	-0.7359
01A-02A	2.741(4)	2.734(5)	2.725(6)	2.733(6)	2.733(7)	2.727(7)	
01A-03A	2.700(4)	2.690(5)	2.676(6)	2.670(6)	2.673(7)	2.653(7)	
01A-03A'	2.634(4)	2.630(5)	2.629(5)	2.633(6)	2.641(7)	2.628(7)	
02A-03A	2.514(4)	2.529(6)	2.523(6)	2.526(7)	2.535(7)	2.529(8)	
02A-03A'	2.686(4)	2.671(6)	2.661(6)	2.662(7)	2.646(8)	2.650(8)	
03A-03A'	2.6309(6)	2.6352(6)	2.6406(4)	2.6503(4)	2.6562(3)	2.6600(1)	
Mean	2.651	2.648	2.642	2.646	2.647	2.641	
01B-02B	2.739(4)	2.738(5)	2.737(6)	2.742(6)	2.749(7)	2.738(8)	
01B-03B	2.635(4)	2.639(5)	2.635(6)	2.641(6)	2.639(7)	2.653(8)	
01B-03B'	2.638(4)	2.635(5)	2.627(6)	2.630(6)	2.616(7)	2.620(8)	
02B-03B	2.597(5)	2.584(6)	2.597(7)	2.575(8)	2.590(9)	2.573(10)	
02B-03B'	2.662(4)	2.654(5)	2.645(6)	2.636(6)	2.629(7)	2.618(8)	
03B-03B'	2.756(2)	2.743(2)	2.737(2)	2.718(2)	2.716(3)	2.706(3)	
Mean	2.671	2.662	2.663	2.657	2.657	2.651	

* Errors in parentheses are one standard deviation.

TABLE 5. Interatomic Angles (°) in Tetrahedral Chains of Orthoferrosilite at Several Temperatures

Atoms	24°C	400°C	600°C	800°C	900°C	980°C
01A -SiA-02A	116.71(18)*	116.73(23)	116.24(25)	116.20(29)	116.47(32)	116.64(34)
01A - -03A	111.58(17)	110.71(21)	110.38(22)	109.67(24)	109.47(26)	108.94(29)
01A - -03A'	108.50(17)	108.88(20)	108.58(22)	108.81(24)	108.99(26)	108.32(29)
02A - -03A	100.97(16)	101.56(21)	102.17(24)	102.03(27)	102.64(29)	102.87(32)
02A - -03A'	112.03(17)	111.69(22)	111.42(25)	111.37(28)	110.60(37)	110.95(32)
03A - -03A'	106.46(12)	106.67(15)	107.63(16)	108.36(18)	108.26(19)	108.79(20)
Mean	109.38	109.37	109.40	109.41	109.42	109.42
01B -SiB-02B	116.64(18)	116.65(22)	116.73(25)	117.21(28)	117.18(31)	116.76(35)
01B - -03B	106.56(17)	106.85(21)	106.93(24)	107.42(27)	107.07(28)	108.10(32)
01B - -03B'	106.94(17)	107.23(21)	107.13(23)	107.55(26)	107.34(28)	108.00(31)
02B - -03B	105.43(17)	104.88(23)	105.54(25)	104.68(29)	104.99(31)	104.21(35)
02B - -03B'	109.52(17)	109.65(21)	109.08(24)	109.07(27)	108.96(29)	108.72(33)
03B - -03B'	111.80(13)	111.61(16)	111.47(18)	110.87(19)	111.31(20)	111.00(23)
Mean	109.48	109.48	109.48	109.47	109.48	109.47
SiA -03A-SiA	138.87(27)	139.76(25)	141.26(28)	141.98(32)	141.95(33)	143.39(36)
SiB -03B-SiB	131.59(20)	133.87(26)	135.18(28)	137.83(34)	139.55(36)	140.08(40)
03A'-03A-03A''	190.89(28)	187.43(37)	185.26(41)	183.99(48)	182.37(52)	180.68(56)
03B'-03B-03B''	143.76(24)	146.97(31)	149.00(36)	154.07(45)	155.75(52)	158.85(60)

* Errors in parentheses are one standard deviation.

whereas the bridging oxygens connect individual tetrahedra in the silicate chains.

Thermal expansion mechanisms in pyroxenes

In recent years, numerous pyroxene structures have been refined using high-temperature data

(Brown *et al.*, 1972; Smyth and Burnham, 1972; Cameron *et al.*, 1973; Smyth, 1973; Smyth, 1974a). In all of these studies thermal expansion of the silicate tetrahedra was much less than that of the *M1* and *M2* polyhedra. Volumes of the tetrahedra changed only slightly with increasing temperature, and in addition,

TABLE 6. Fe-O and O-O Interatomic Distances in Fe Coordination Polyhedra in Orthoferrosilite at Several Temperatures

Atom	24°C	400°C	Fe-O distances (Å)				MTEC** ($\times 10^{-5}$)	
			600°C	800°C	900°C	980°C		
Fe1-01A	2.195(3)*	2.214(4)	2.228(4)	2.238(5)	2.241(5)	2.254(6)	2.657	
-01A'	2.085(3)	2.084(4)	2.090(4)	2.089(4)	2.093(5)	2.101(5)	0.665	
-01B	2.194(3)	2.231(4)	2.250(5)	2.269(5)	2.274(5)	2.289(6)	4.368	
-01B'	2.124(3)	2.110(4)	2.112(4)	2.109(5)	2.109(5)	2.105(5)	-0.817	
-02A	2.090(3)	2.110(4)	2.123(5)	2.127(5)	2.128(6)	2.134(6)	2.117	
-02B	2.124(3)	2.137(4)	2.134(5)	2.131(5)	2.133(5)	2.136(6)	0.378	
Mean	2.135	2.148	2.156	2.161	2.163	2.170	1.591	
Fe2-01A	2.158(3)	2.170(4)	2.164(4)	2.160(5)	2.162(5)	2.160(6)	-0.035	
-01B	2.129(3)	2.131(4)	2.139(5)	2.137(5)	2.135(5)	2.140(6)	0.477	
-02A	2.024(3)	2.018(4)	2.020(5)	2.018(5)	2.029(5)	2.014(6)	-0.149	
-02B	1.994(3)	1.985(4)	1.993(5)	1.994(5)	1.990(5)	2.000(6)	0.235	
-03A	2.460(3)	2.513(4)	2.556(5)	2.581(5)	2.598(6)	2.628(6)	6.879	
-03B	2.600(3)	2.699(4)	2.770(5)	2.887(5)	2.960(6)	3.016(7)	16.986	
-03B'	3.097(3)	3.060(4)	3.036(5)	2.971(6)	2.950(6)	2.900(7)	-6.314	
Mean (6)	2.228	2.253	2.274	2.296	2.311	2.326	4.592	
(7)	2.352	2.368	2.383	2.393	2.403	2.408	2.546	
			O-O distances (Å)					
Fe1 Octahedron	24°C	400°C	600°C	800°C	900°C	980°C		
01A -01A'	3.083(3)	3.087(4)	3.103(5)	3.110(5)	3.113(6)	3.125(6)		
01A -02A	3.119(4)	3.137(6)	3.154(6)	3.176(7)	3.183(8)	3.199(8)		
01A' -02A	3.103(5)	3.131(6)	3.168(6)	3.170(7)	3.174(8)	3.198(8)		
01A -01B	2.849(4)	2.883(5)	2.899(5)	2.912(6)	2.912(6)	2.929(7)		
01A' -01B	2.932(4)	2.936(5)	2.946(5)	2.947(5)	2.945(6)	2.958(6)		
01A' -01B'	2.932(4)	2.936(5)	2.946(5)	2.947(5)	2.945(6)	2.958(6)		
01A' -02B	2.838(4)	2.851(5)	2.857(6)	2.858(7)	2.857(7)	2.875(8)		
02A -01B'	2.907(4)	2.909(6)	2.922(5)	2.909(7)	2.910(7)	2.897(5)		
02A -02B	2.947(4)	2.993(6)	3.015(4)	3.025(7)	3.039(7)	3.053(4)		
01B -01B'	3.054(3)	3.081(4)	3.089(5)	3.112(5)	3.123(6)	3.131(7)		
01B -02B	3.235(4)	3.264(6)	3.253(4)	3.263(7)	3.257(8)	3.261(9)		
01B' -02B	3.192(5)	3.197(6)	3.188(5)	3.184(7)	3.194(8)	3.180(9)		
Fe2 Polyhedron	24°C	400°C	600°C	800°C	900°C	980°C		
01A-02A	2.925(5)	2.943(6)	2.949(6)	2.963(7)	2.983(8)	2.967(9)		
01A-03A	2.634(4)	2.630(5)	2.629(5)	2.633(6)	2.641(7)	2.623(7)		
02A-03A	2.514(4)	2.529(6)	2.523(6)	2.526(7)	2.535(7)	2.529(8)		
01A-01B	2.849(4)	2.883(5)	2.899(5)	2.912(6)	2.912(6)	2.929(7)		
01A-02B	2.838(4)	2.851(5)	2.857(6)	2.858(7)	2.857(7)	2.875(8)		
02A-01B	2.908(5)	2.909(6)	2.922(6)	2.909(7)	2.910(7)	2.897(8)		
02A-03B	3.093(5)	3.132(6)	3.153(6)	3.191(7)	3.223(8)	3.232(9)		
03A-02B	3.339(4)	3.331(6)	3.346(6)	3.350(7)	3.352(7)	3.357(8)		
03A-03B	2.950(4)	2.999(5)	3.039(6)	3.085(6)	3.129(6)	3.147(7)		
01B-02B	3.015(5)	3.021(6)	3.030(7)	3.036(7)	3.021(8)	3.038(9)		
01B-03B	3.396(5)	3.451(6)	3.495(7)					
02B-03B	2.662(4)	2.654(5)	2.645(6)	2.636(7)	2.629(7)	2.618(8)		

* Error in parentheses represents one standard deviation.

** MTEC: Mean thermal expansion coefficient. See text of paper for explanation.

TABLE 7. Interatomic Angles ($^{\circ}$) in Fe Coordination Polyhedra in Orthoferrosilite at Several Temperatures

Atom	24 $^{\circ}$ C	400 $^{\circ}$ C	600 $^{\circ}$ C	800 $^{\circ}$ C	900 $^{\circ}$ C	980 $^{\circ}$ C
01A -M1-01A'	92.13(12)*	91.77(14)	91.82(15)	91.84(17)	91.76(19)	91.62(20)
01A - -02A	93.37(12)	92.97(15)	93.44(16)	93.36(18)	93.49(20)	93.57(21)
01A' - -02A	96.03(12)	96.58(15)	96.95(17)	97.52(18)	97.50(20)	98.06(22)
01A - -01B	80.93(11)	80.84(13)	80.69(14)	80.49(15)	80.34(16)	80.29(17)
01A - -01B'	85.49(12)	85.46(14)	85.46(16)	85.31(16)	85.15(18)	85.42(20)
01A' - -01B	86.47(12)	85.66(14)	85.44(15)	84.97(17)	84.68(18)	84.62(20)
01A' - -02B	84.82(12)	84.96(16)	85.13(17)	85.23(19)	85.05(20)	85.47(23)
02A - -01B'	87.29(12)	87.15(15)	87.25(17)	86.75(19)	86.75(20)	86.23(23)
02A - -02B	88.78(13)	89.63(15)	90.18(17)	90.57(19)	91.02(20)	91.33(22)
01B - -01B'	90.01(11)	90.35(14)	90.13(16)	90.51(17)	90.79(18)	90.82(20)
01B - -02B	97.03(12)	96.65(15)	95.79(17)	95.67(18)	95.24(19)	94.91(22)
01B' - -02B	97.45(13)	97.66(15)	97.34(18)	97.36(19)	97.72(20)	97.15(23)
01A-M2-02A	88.72(13)	89.24(15)	89.58(17)	90.27(19)	90.72(20)	90.53(22)
01A- -03A	110.27(11)	111.12(13)	111.34(14)	111.85(16)	112.45(17)	112.29(19)
02A- -03A	67.39(12)	66.83(14)	65.70(16)	65.30(17)	65.11(18)	64.46(20)
01A- -01B	83.29(11)	84.17(13)	84.70(15)	85.34(16)	85.34(17)	85.87(19)
01A- -02B	86.16(13)	86.53(16)	86.73(17)	86.83(18)	86.86(20)	87.37(22)
02A- -01B	88.88(13)	89.01(16)	89.20(17)	88.84(19)	88.65(20)	88.37(22)
02A- -03B	83.02(12)	81.83(15)	80.68(17)	79.00(18)	121.23(19)	120.48(21)
03A- -02B	111.26(12)	111.21(15)	112.21(16)	112.50(18)	113.15(19)	113.76(22)
03A- -03B	71.30(10)	70.14(12)	69.46(13)	68.43(14)	65.95(14)	66.12(16)
01B- -02B	93.95(12)	94.38(16)	94.25(18)	94.53(20)	94.11(22)	94.34(24)
01B- -03B	91.31(11)	90.41(13)	89.85(15)	89.25(16)	88.60(18)	88.39(20)
02B- -03B	102.38(11)	102.72(14)	103.33(16)	104.20(17)	104.65(19)	105.22(22)

*

Errors in parentheses are one standard deviation.

the volume of the *M2* polyhedron (generally occupied by larger cations such as Ca, Na, Fe^{2+}) showed a higher rate of increase than the *M1* polyhedron (occupied by atoms such as Mg, Al, Fe^{3+} , Fe^{2+}). This differential thermal expansion between the tetrahedra and polyhedra determines to a large degree how the structures behave with increasing temperature. Structural adaptations (Cameron *et al.*, 1973) necessary to maintain the fit between the tetrahedral chains and the octahedral strips include: (1) stretching of the silicate chains (increase of O3-O3-O3 angle), (2) distortion of the silicate tetrahedra, and (3) increase in out-of-plane tilting of tetrahedra as a result of movement of the O2 atoms farther from the *bc* plane which contains the O3 atoms.

Topology of the *Pbca*, *P2₁/c* and *C2/c* structures

Thompson (1970) discussed pyroxene architecture based on ideal close-packing of oxygen atoms, *i.e.*, regular tetrahedra and octahedra with equal-length edges. In these "ideal" models, the basal triangle of an individual tetrahedron or octahedron is assumed to be parallel to the *bc* plane of the unit cell. Thompson (1970) pointed out that there are two possible orientations of a tetrahedral chain with re-

spect to the *M1* octahedral strip to which it is connected through common O1 oxygen atoms. Thompson called these *O* or *S* rotations because in real silicate structures the orientations of the silicate chains are intermediate between the *O* and *S* extremes. In this paper, we use *O* or *S* orientation when speaking of ideal structures and *O* or *S* rotation to indicate the direction of rotation in real structures. In an *O* orientation or rotation, the basal triangles of the tetrahedra in the chain point in a direction *opposite* to the triangles on the top of the *M1* octahedra to which they are linked (Fig. 2a). In an *S* orientation, the tetrahedral triangles are directed in the *same* way as the triangular faces of the octahedra (Fig. 2b). These two orientations correspond to cubic close packing (*O* orientations) or hexagonal close packing (*S* orientations) of the oxygen atoms.

Although the concept of *O* and *S* orientations is convenient for describing the two possibilities shown in Figure 2, additional relationships occur when larger segments of the structure are examined. Not only is it possible to attach tetrahedral chains to the tops and bottoms of octahedral strips in two different ways, but it is also possible to attach them laterally in different ways. Following the Thompson theme, we

TABLE 8. Amplitudes and Orientations of Major Axes of Thermal Ellipsoids

Atom	Ellipsoid axis (r_i)		24°C	400°C	600°C	800°C	900°C	980°C
Fe 1	r_1	rms*	.064(2)**	.104(2)	.116(2)	.130(2)	.136(2)	.145(2)
		a^\dagger	33 (7)	58 (5)	58 (3)	63 (2)	57 (2)	60 (3)
		b^\dagger	94 (5)	93 (4)	99 (3)	99 (3)	89 (3)	94 (3)
	r_2	c^\dagger	57 (7)	32 (5)	33 (3)	29 (3)	33 (2)	30 (3)
		rms	.075(2)	.118(2)	.139(2)	.157(2)	.165(2)	.176(2)
		a	57 (8)	36 (6)	32 (3)	39 (8)	33 (2)	30 (3)
	r_3	b	79 (7)	70 (8)	86 (11)	114 (11)	89 (13)	89 (11)
		c	144 (8)	119 (5)	122 (4)	119 (3)	123 (2)	120 (3)
		rms	.088(2)	.128(2)	.146(2)	.164(2)	.172(2)	.185(2)
	r_1	a	93 (5)	106 (7)	88 (10)	115 (10)	90 (25)	89 (10)
		b	12 (7)	20 (8)	9 (5)	154 (11)	179 (26)	5 (4)
		c	79 (6)	78 (5)	81 (7)	87 (7)	89 (14)	86 (7)
Fe 2	r_1	rms	.067(2)	.106(2)	.124(2)	.141(2)	.149(2)	.156(2)
		a	49 (3)	51 (2)	49 (1)	50 (1)	52 (1)	47 (1)
		b	86 (3)	90 (2)	90 (2)	85 (2)	92 (2)	83 (2)
	r_2	c	41 (3)	39 (2)	41 (1)	41 (1)	38 (1)	44 (1)
		rms	.090(2)	.142(2)	.167(2)	.189(2)	.199(2)	.212(2)
		a	51 (4)	60 (3)	61 (3)	67 (4)	66 (5)	72 (4)
	r_3	b	59 (5)	40 (4)	40 (5)	34 (5)	30 (6)	32 (6)
		c	126 (4)	114 (3)	115 (3)	114 (3)	107 (4)	116 (4)
		rms	.104(2)	.157(2)	.182(2)	.203(2)	.214(2)	.228(2)
	r_1	a	115 (4)	127 (3)	125 (3)	131 (3)	132 (3)	132 (3)
		b	31 (5)	50 (4)	50 (5)	56 (5)	60 (6)	59 (6)
		c	73 (4)	61 (2)	60 (3)	60 (3)	57 (2)	57 (3)
Si A	r_1	rms	.061(2)	.090(3)	.104(4)	.110(4)	.117(3)	.124(4)
		a	16 (18)	157 (21)	30 (22)	22 (14)	11 (6)	96 (26)
		b	89 (5)	105 (7)	71 (5)	75 (5)	79 (5)	73 (6)
	r_2	c	73 (18)	73 (31)	68 (26)	74 (15)	86 (9)	18 (6)
		rms	.070(3)	.095(3)	.109(3)	.120(3)	.134(3)	.131(4)
		a	74 (18)	106 (29)	66 (25)	71 (15)	84 (9)	170 (16)
	r_3	b	91 (7)	100 (9)	91 (9)	100 (6)	101 (7)	99 (8)
		c	164 (18)	162 (30)	156 (25)	158 (12)	168 (7)	94 (24)
		rms	.095(3)	.125(3)	.137(3)	.155(3)	.160(3)	.173(4)
	r_1	a	90 (5)	73 (5)	73 (5)	79 (4)	80 (4)	83 (5)
		b	779 (7)	163 (5)	161 (5)	161 (4)	165 (5)	161 (4)
		c	89 (6)	86 (6)	81 (6)	75 (5)	78 (7)	73 (4)
Si B	r_1	rms	.057(4)	.084(3)	.100(3)	.109(4)	.115(4)	.125(4)
		a	18 (7)	19 (8)	35 (9)	37 (6)	33 (6)	30 (7)
		b	104 (8)	94 (6)	95 (6)	110 (5)	104 (5)	102 (7)
	r_2	c	80 (8)	71 (7)	55 (10)	60 (6)	61 (5)	63 (6)
		rms	.076(4)	.103(3)	.113(3)	.133(3)	.141(3)	.149(4)
		a	87 (10)	71 (8)	59 (10)	55 (7)	57 (6)	60 (7)
	r_3	b	118 (21)	68 (11)	108 (7)	81 (12)	76 (15)	60 (11)
		c	152 (20)	150 (10)	143 (10)	143 (9)	144 (11)	135 (10)
		rms	.083(3)	.117(3)	.136(3)	.146(3)	.152(3)	.164(4)
	r_1	a	107 (7)	93 (6)	104 (5)	79 (9)	85 (10)	94 (8)
		b	148 (19)	22 (11)	162 (7)	22 (7)	20 (11)	33 (10)
		c	64 (21)	68 (10)	78 (6)	71 (11)	70 (14)	57 (10)
O1A	r_1	rms	.059(10)	.090(8)	.107(8)	.091(10)	.128(9)	.126(10)
		a	12 (8)	7 (10)	174 (9)	151 (6)	167 (7)	170 (11)
		b	83 (15)	85 (8)	96 (9)	98 (4)	102 (6)	95 (7)
	r_2	c	80 (11)	84 (10)	90 (6)	63 (6)	87 (12)	81 (10)
		rms	.088(9)	.126(8)	.141(8)	.150(8)	.161(9)	.167(10)
		a	90 (16)	83 (10)	90 (11)	118 (7)	95 (12)	100 (11)
	r_3	b	35 (18)	107 (21)	96 (31)	85 (10)	83 (11)	73 (12)
		c	125 (18)	161 (21)	174 (32)	151 (7)	171 (12)	160 (12)
		rms	.107(8)	.144(7)	.154(7)	.191(7)	.199(8)	.206(9)
	r_1	a	102 (8)	87 (8)	84 (9)	95 (6)	101 (6)	92 (6)
		b	56 (18)	162 (20)	172 (24)	10 (6)	14 (8)	17 (11)
		c	37 (18)	72 (21)	84 (32)	82 (9)	82 (12)	73 (12)

TABLE 8, Continued

Atom	Ellipsoid axis (r_i)	24°C	400°C	600°C	800°C	900°C	980°C	
02A	rms	.067(11)	.106(9)	.129(9)	.147(9)	.145(10)	.150(10)	
	r_1	a	83 (15)	134 (8)	117 (7)	47 (8)	63 (6)	54 (7)
		b	116 (17)	136 (8)	153 (7)	44 (9)	34 (11)	37 (6)
		c	27 (13)	87 (16)	89 (18)	84 (18)	71 (17)	83 (17)
	r_2	rms	.087(9)	.129(8)	.150(8)	.170(8)	.171(9)	.170(10)
		a	131 (11)	104 (18)	99 (14)	94 (20)	88 (12)	80 (15)
		b	135 (16)	80 (16)	86 (18)	77 (17)	70 (16)	89 (15)
	r_3	c	105 (19)	163 (18)	171 (11)	167 (18)	160 (17)	170 (15)
		rms	.118(7)	.150(7)	.184(7)	.192(8)	.215(8)	.216(9)
a		138 (10)	132 (9)	151 (7)	136 (8)	153 (6)	37 (7)	
03A	r_1	b	56 (9)	47 (8)	63 (6)	49 (9)	64 (6)	127 (6)
		c	68 (8)	73 (17)	81 (10)	78 (19)	83 (9)	83 (12)
		rms	.071(10)	.090(10)	.092(11)	.105(11)	.116(11)	.115(14)
	r_2	a	44 (44)	66 (21)	76 (17)	114 (13)	63 (21)	91 (17)
		b	80 (22)	71 (6)	62 (4)	70 (4)	70 (6)	60 (3)
		c	48 (37)	31 (15)	32 (7)	32 (9)	34 (15)	30 (3)
	r_3	rms	.080(9)	.110(8)	.119(8)	.140(9)	.137(10)	.144(10)
		a	49 (44)	24 (21)	14 (17)	156 (13)	27 (21)	176 (4)
		b	117 (12)	101 (8)	97 (9)	101 (5)	103 (8)	86 (9)
r_3	c	127 (39)	111 (19)	102 (15)	111 (12)	113 (19)	93 (16)	
	rms	.123(7)	.186(6)	.214(7)	.250(8)	.255(8)	.274(10)	
	a	102 (7)	93 (4)	91 (4)	89 (3)	93 (3)	94 (3)	
01B	r_1	b	151 (8)	158 (4)	151 (3)	157 (3)	156 (3)	150 (3)
		c	64 (8)	68 (4)	61 (3)	67 (3)	67 (3)	60 (3)
		rms	.054(12)	.085(9)	.113(9)	.103(10)	.116(10)	.145(10)
	r_2	a	29 (7)	8 (8)	19 (8)	15 (6)	24 (6)	25 (10)
		b	76 (7)	86 (7)	74 (6)	77 (5)	71 (5)	74 (8)
		c	66 (8)	83 (8)	79 (14)	82 (6)	76 (7)	71 (13)
	r_3	rms	.099(8)	.132(7)	.140(7)	.166(7)	.175(8)	.179(9)
		a	74 (10)	83 (8)	82 (14)	80 (8)	72 (9)	74 (14)
		b	63 (16)	90 (26)	81 (10)	98 (18)	98 (17)	78 (18)
r_3	c	148 (12)	173 (8)	167 (12)	168 (15)	160 (14)	160 (13)	
	rms	.120(7)	.147(7)	.181(7)	.189(8)	.199(8)	.204(9)	
	a	113 (7)	86 (8)	107 (6)	79 (6)	74 (8)	109 (9)	
02B	r_1	b	31 (14)	176 (7)	18 (7)	165 (10)	159 (9)	21 (12)
		c	71 (15)	90 (26)	83 (10)	81 (18)	77 (18)	83 (18)
		rms	.082(9)	.088(10)	.111(10)	.123(10)	.125(11)	.171(10)
	r_2	a	51 (54)	56 (7)	56 (6)	54 (6)	58 (6)	125 (7)
		b	132 (21)	132 (5)	136 (7)	136 (5)	137 (6)	36 (11)
		c	67 (94)	70 (8)	65 (9)	69 (10)	64 (9)	84 (55)
	r_3	rms	.086(8)	.135(8)	.155(8)	.163(8)	.172(9)	.181(10)
		a	65 (69)	53 (11)	82 (14)	69 (10)	70 (10)	93 (31)
		b	97 (65)	94 (10)	114 (12)	100 (9)	107 (9)	84 (43)
r_3	c	154 (87)	143 (10)	154 (10)	156 (11)	153 (9)	174 (51)	
	rms	.109(7)	.163(7)	.178(7)	.209(8)	.216(8)	.238(9)	
	a	49 (13)	55 (9)	145 (7)	44 (6)	39 (6)	35 (7)	
03B	r_1	b	43 (13)	43 (5)	124 (9)	48 (5)	51 (5)	55 (7)
		c	78 (16)	69 (11)	83 (15)	81 (8)	84 (9)	89 (8)
		rms	.066(11)	.085(10)	.119(9)	.128(10)	.139(10)	.164(10)
	r_2	a	96 (23)	97 (9)	114 (21)	86 (19)	81 (17)	102 (61)
		b	80 (10)	63 (5)	74 (15)	55 (5)	61 (4)	72 (23)
		c	12 (16)	28 (5)	29 (11)	36 (7)	31 (9)	22 (17)
	r_3	rms	.085(8)	.127(7)	.135(8)	.150(9)	.163(9)	.171(10)
		a	173 (22)	167 (11)	144 (17)	15 (7)	17 (11)	160 (39)
		b	88 (17)	103 (11)	124 (10)	81 (12)	82 (9)	109 (22)
r_3	c	97 (23)	91 (10)	102 (21)	101 (16)	105 (16)	95 (62)	
	rms	.105(7)	.156(7)	.185(7)	.230(8)	.239(8)	.263(9)	
	a	94 (16)	79 (11)	65 (6)	76 (4)	76 (5)	74 (5)	
r_3	b	170 (10)	150 (6)	142 (6)	143 (3)	150 (4)	153 (4)	
	c	80 (10)	62 (5)	64 (5)	57 (3)	64 (4)	69 (4)	

* rms: root mean square amplitude (\AA).

** Errors in parentheses are one standard deviation.

† a, b, c represent angles ($^\circ$) of r_i with cell edges a, b, c, respectively.

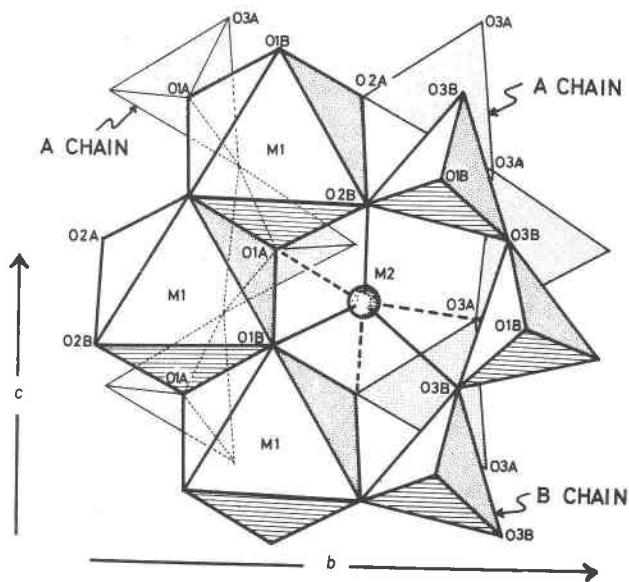


FIG. 1. Projection along a^* of part of the orthoferrosilite structure.

define N (negative) and P (positive) orientations as shown in Figure 3. In the N configuration (Fig. 3a), the basal triangles of the lateral tetrahedral chains point opposite to the triangles of the octahedra to which they are joined through common O2 oxygen atoms. In Figure 3c the orientations are both P , and in Figure 3b one of each type is shown.³ One aspect of N and P orientations is that the combinations $\frac{N}{N}$, $\frac{P}{N}$, and $\frac{P}{P}$ result in different geometries and size limitations for the $M2$ site. Although in ideal structures the $M2$ site is octahedral, the $\frac{P}{P}$ configuration is the most stable because tetrahedra and octahedra do not share edges, and they adjust their shape and position relatively independently from each other. In the $\frac{P}{N}$ and $\frac{N}{N}$ configurations, one and two edges are shared, respectively. Each N occurring in this notation thus indicates an edge shared between an octahedron and a tetrahedron. Because of constraints due to edge-sharing, $M2$ sites in real structures with $\frac{P}{P}$ relationships are able to accept larger cations and, consequently, have larger volumes.

In order to preserve close-packing relationships in the ideal structures, only combinations of O with P and S with N are possible. For example, a chain with O orientation could not be attached to the upper side

³ J. J. Papike, C. T. Prewitt, S. Sueno, and M. Cameron (1973) reviewed and discussed the topological differences of pyroxenes of several different space group symmetries using "ideal" models. In that paper symbols such as $\frac{U}{D} \cdot \frac{P}{U}$ were introduced to describe the variation of the oxygen configuration around the $M2$ site in the various pyroxene structures.

of the octahedra in Figure 3a without violating the close packing arrangement [Thompson's (1970) parity violation]. However, in real silicate structures distortions permit parity violations to occur, and the $Pbca$ orthopyroxene structure has a combination of O and N rotations (Fig. 4c).

"I-beam" diagrams for $C2/c$, $P2_1/c$, and $Pbca$ silicate pyroxenes with S , O , P , and N symbolism for describing the rotational modes of tetrahedral chains and the coordination of $M2$ sites are shown in Figure 4. Each "I-beam" represents a tetrahedral-octahedral-tetrahedral unit in a real pyroxene structure. The (+) or (-) refers to the "skew" or "tilt" direction of the $M1$ octahedra. The $C2/c$ model has the octahedral sequence +, +, +, ... and the tetrahedral chains all have O and P rotations. $C2/c$ symmetry is also compatible with S and N rotations, but this results in the $M2$ octahedron sharing two edges. The octahedral stacking sequence in the $P2_1/c$ model is +, +, +, ..., but there are two crystallographically distinct tetrahedral chains; these chains occur in combinations of $S-N$ and $O-P$ rotation. The octahedral stacking sequence of the $Pbca$ model is +, +, -, -, +, +, ..., and two symmetrically distinct chains, the A and B chains, are O rotated with both P and N combinations.

Thermal structural expansion in orthoferrosilite

Mean Si-O bond lengths (Table 4, Fig. 5) and volumes (Table 9) of both the SiA and SiB tetrahedra decrease slightly with increasing temperature. The changes are regular, and over the temperature inter-

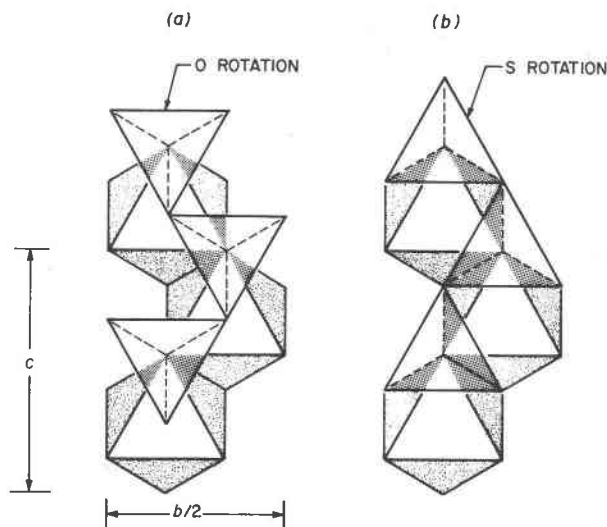


FIG. 2. Portion of the pyroxene structure showing O and S orientations of the tetrahedral chains (after Thompson, 1970).

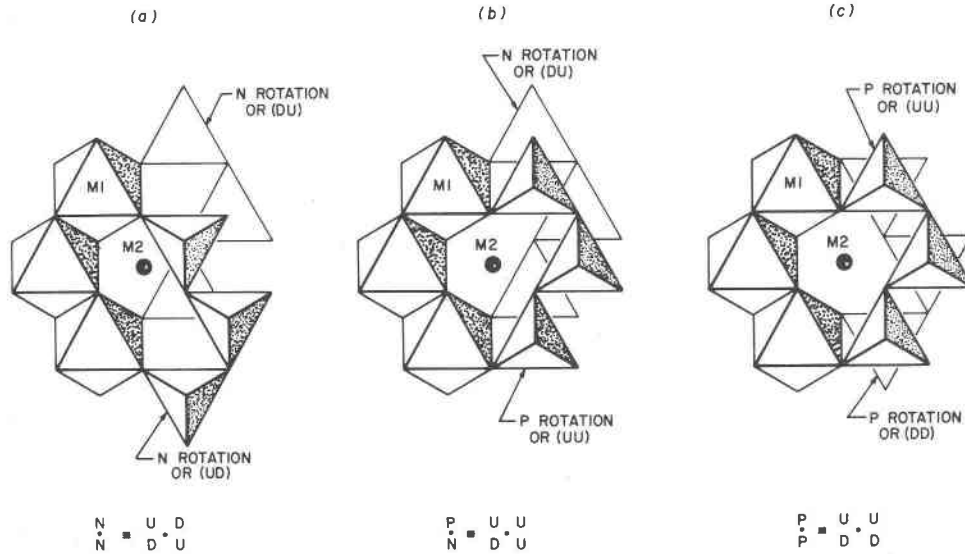


FIG. 3. a. $\frac{N}{N}$ tetrahedral chain configuration around the $M2$ site. Note that the tetrahedra and $M2$ octahedron share two edges.
 b. $\frac{P}{N}$ tetrahedral chain configuration around the $M2$ site. Note that the tetrahedra and $M2$ octahedron share one edge.
 c. $\frac{P}{P}$ tetrahedral chain configuration around the $M2$ site. Note that the tetrahedra and $M2$ octahedron do not share edges.

val studied the decreases are approximately equal to four times the standard deviation of the mean Si-O bond length at room temperature. The decrease observed is larger for the larger SiB tetrahedra (0.012\AA vs 0.007\AA), thus reducing the size difference between the two tetrahedra. This is consistent with other pyroxenes where the larger silicate tetrahedra occur in the more kinked chains. The O3-O3 dis-

tances behave differently in the two chains: a decrease of 0.05\AA is observed in the larger SiB tetrahedron and an increase of 0.029\AA occurs in the SiA tetrahedron. These contrasting changes, coupled with different rates of straightening of the A and B chains, are important in maintaining the fit between the silicate chains and octahedral strips with increasing temperature.

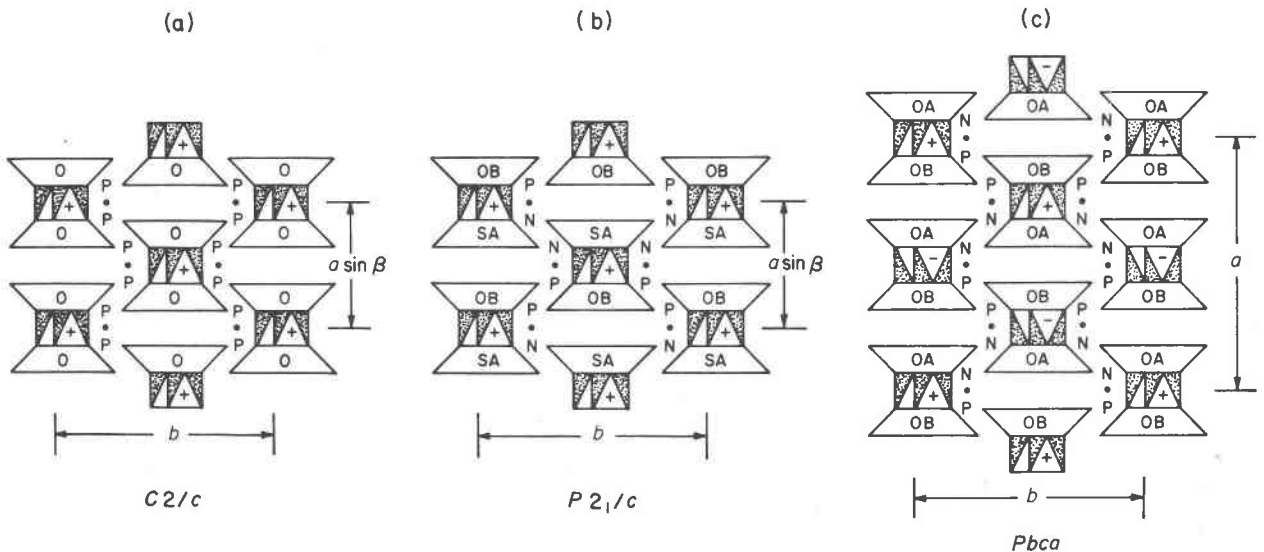


FIG. 4. "I-beam" diagrams of three pyroxene structural types with N and P symbolism. See text of paper for explanation.

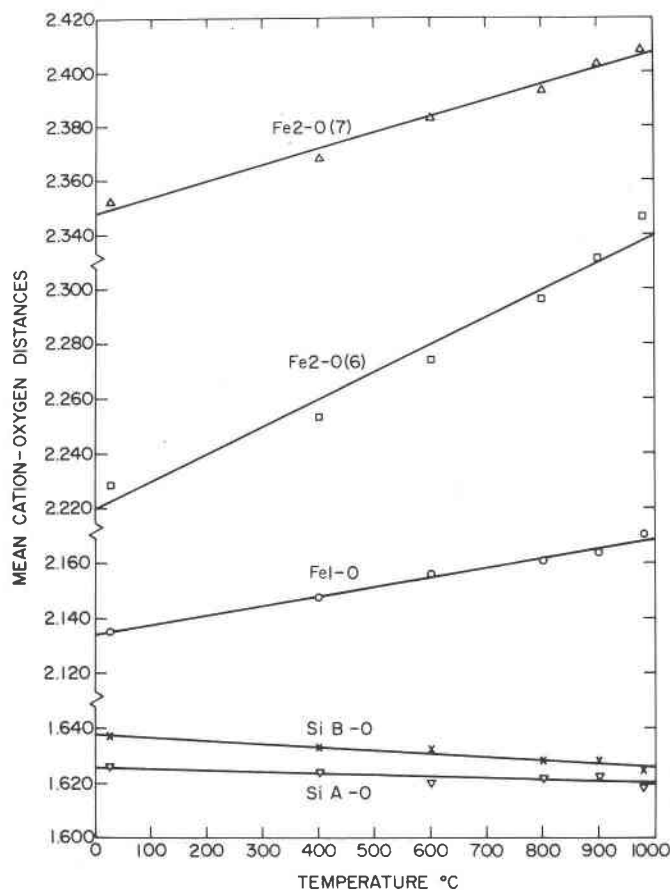


FIG. 5. Variation of mean cation-oxygen distances in orthoferrosilite with increasing temperature.

The FeI and Fe2 polyhedra both expand significantly with increasing temperature (Tables 6, 9, and Fig. 5). At room temperature FeI is coordinated by four oxygens within 2.125Å and by two at approximately 2.195Å. With increasing temperature this coordination is maintained, but the two longest bonds, FeI-O1A and FeI-O1B, exhibit slightly higher rates of increase (Fig. 6). Changes in individual bond lengths result in FeI-O1A' and FeI-O1B' becoming almost equivalent at temperatures close to 980°C.

TABLE 9. Cation Polyhedral Volume Expansion in Orthoferrosilite

	24°C	400°C	600°C	800°C	900°C	980°C	MTEC*
FeI	12.804	13.039	13.189	13.270	13.3118	13.432	5.0133
Fe2	16.851	17.240	17.569	17.837	18.074	18.175	8.4033
SiA	2.182	2.180	2.165	2.174	2.177	2.162	-0.671
SiB	2.233	2.221	2.216	2.199	2.198	2.187	-2.0736

* See text of paper for explanation.

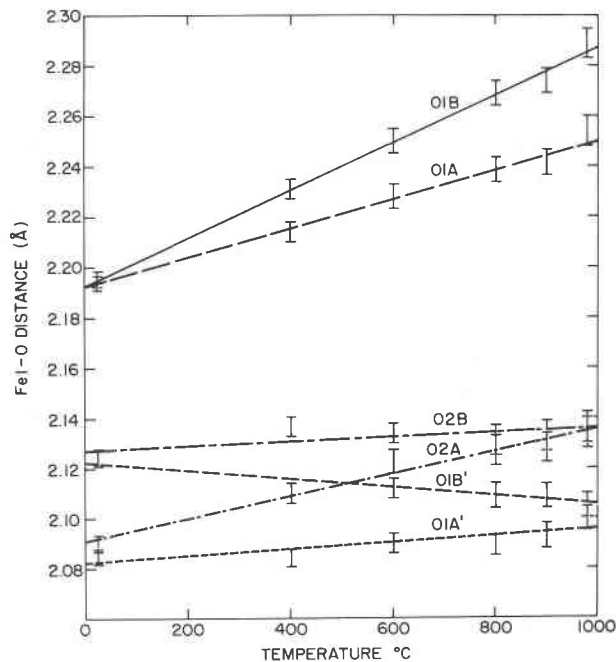


FIG. 6. Variation of individual FeI-O distances in orthoferrosilite with increasing temperature.

The same is true for the FeI-O2A and FeI-O2B bonds.

At room temperature the Fe2 cation is coordinated by six oxygens in a very distorted octahedral arrangement: O1A, O1B, O2A, O2B are within 2.16Å, O3A is at 2.46Å, and O3B at 2.60Å. The next nearest oxygen, O3B' is at 3.10Å. With increasing temperature, the four short bonds remain relatively constant. However, as a result of the behavior of the three O3 atoms, the coordination number of the Fe2 cation (arbitrarily chosen as the number of oxygen atoms less than 3.00Å distant) changes from six at 24°C to seven between 600° and 800°C, and back to six at higher temperatures. The change in coordination is related to the thermal expansion of the Fe2 polyhedron and the concomitant straightening of the tetrahedral chains with increasing temperature (Fig. 7). As the B tetrahedral chain straightens, O3B' moves closer to, and O3B farther from, Fe2. At approximately 675°C the two O3B oxygens are at an equal distance from Fe2, and angle O3B-O3B-O3B approximates 151°. Continued uninking of the B chain moves O3B out of the coordination sphere of Fe2. The A chain, because of its configuration and disposition with respect to the Fe2 site at 24°C, behaves in a slightly different manner with increasing temperature. The same O3A atom remains bonded to Fe2 even at 980°C where the A chain becomes almost

fully extended; the second O3A atom does not enter the coordination sphere over the temperature range studied. In orthoferrosilite, the mean thermal expansion coefficient of the mean Fe–O distances (Table 6) is smaller than that of the Fe2 polyhedron (both as six- and seven-coordinated). The values of the coefficients calculated for mean Fe–O and Fe2–O bonds in orthoferrosilite are significantly larger than that obtained for the six-coordinated Fe²⁺–O bond in

the C2/c hedenbergite structure ($1.05 \times 10^{-5} \text{C}^{-1}$; Cameron *et al.*, 1973).

Tetrahedral chain kinking and tilting

The variation with increasing temperature of the O3–O3–O3 angles of six end-member clinopyroxenes and of the A and B chains in orthoferrosilite and pigeonite are plotted in Figure 7. Both chains in orthoferrosilite straighten with increasing temperature, and at 980°C the A chain is almost completely extended. Throughout the temperature range studied, the B chain (P rotated) remains more kinked than the A chain. The rate of straightening of both chains is greater at higher temperatures. In addition, the tetrahedral chains in orthoferrosilite show a much larger absolute change than those of the C2/c pyroxenes.

The O3–O3–O3 angle in the A chain (Fig. 7) is plotted above 180° and that of the B chain below 180°, to maintain the analogy with the A and B chains in low clinopyroxene despite the fact that both chains are O-rotated in the Pbc_a pyroxene structure (Thompson, 1970; Papike *et al.*, 1973). Figure 7 helps to show how the A and B tetrahedral chains of the Pbc_a or P₂₁/c pyroxenes approach symmetrically equivalent chain angles with increasing temperature and, therefore, the manner in which the M2 coordination changes from $\frac{P}{N}$ to $\frac{P}{P}$ above 980°C.

Thermal expansion of unit cell parameters

The unit-cell parameters of the Pbc_a orthoferrosilite of this study (Table 1) increase regularly with increasing temperature. Assuming linear expansion rates, the mean thermal expansion coefficients, MTEC, decrease in the order $\alpha_c > \alpha_a > \alpha_b$ (Table 10). This order differs from that determined for the C2/c and P₂₁/c pyroxene structures: $\alpha_b > \alpha_{d100} > \alpha_c$ for C2/c clinopyroxenes (Cameron *et al.*, 1973) and $\alpha_c > \alpha_b > \alpha_{d100}$ for P₂₁/c clinopyroxenes (Smyth, 1974a; Ohashi, 1973).⁴

The c axes of both the Pbc_a and the P₂₁/c pyroxenes expand at higher rates than do the c axes of the C2/c pyroxenes. This behavior is related largely to the different magnitudes of straightening or extension of the tetrahedral chains in the three types of structures. The O3–O3–O3 angles in the tetrahedral chains of Pbc_a orthopyroxenes and P₂₁/c clinopyroxenes approach 180° at a rate of 0.6° to

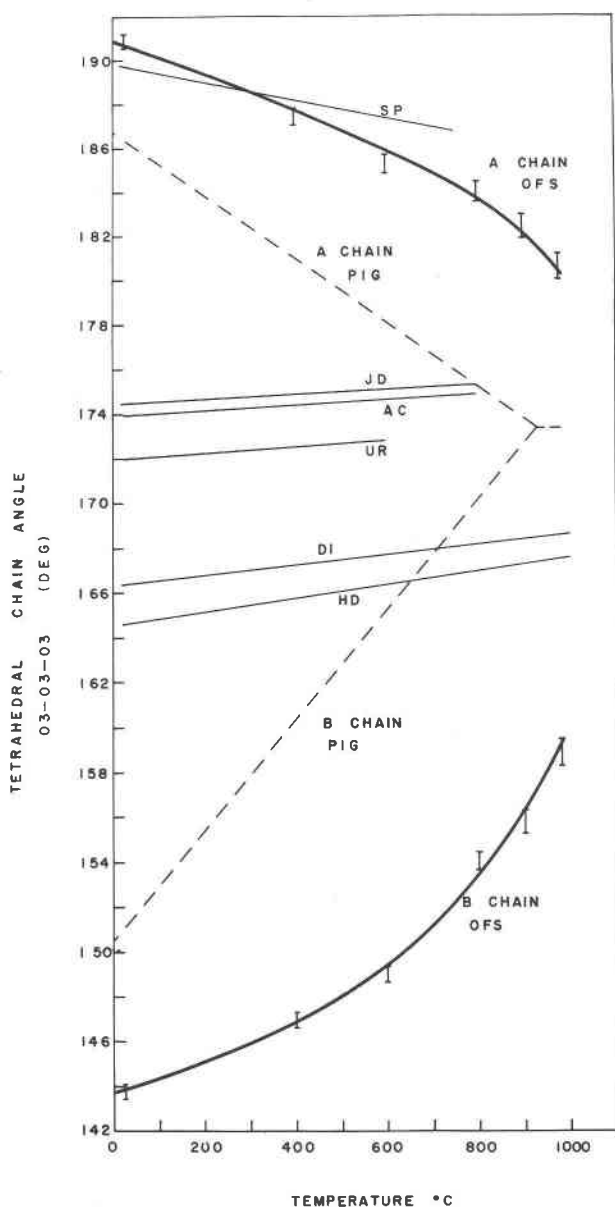


FIG. 7. Variation with increasing temperature of the O3–O3–O3 angles of six end-member clinopyroxenes and of the A and B chains in orthoferrosilite and pigeonite.

⁴ For direct comparison between the orthorhombic and monoclinic systems, the MTEC along a^* was used because this direction is perpendicular to the octahedral layers.

TABLE 10. Mean Thermal Expansion Coefficients ($\times 10^{-4}$) of Pyroxene Cell Parameters

	Pbca		
	Orthoferrosilite** FeSiO ₃ (24°-980°C)	Ferrohypersthene*** Ca _{0.015} Mg _{0.305} Fe _{0.68} SiO ₃ (20°-850°C)	Bronzite† Mg _{0.8} Fe _{0.2} SiO ₃ (25°-1000°C)
a	0.112	0.135	0.164
b	0.109	0.145	0.145
c	0.168	0.154	0.168
v	0.393	0.438	0.477

	C2/c	
	Diopside†† CaMgSi ₂ O ₆ (24°-1000°C)	Hedenbergite†† CaFeSi ₂ O ₆ (24°-1000°C)
a	0.078	0.072
b	0.205	0.176
c	0.065	0.060
d ₁₀₀	0.061	0.048
v	0.333	0.298

	P2 ₁ /c	
	Fs ₈₅ Wo ₁₅ ††† Ca _{0.15} Fe _{0.85} SiO ₃ (24°-500°C)	Clinohypersthene§ Ca _{0.015} Mg _{0.305} Fe _{0.68} SiO ₃ (20°-700°C)
a	0.189	0.162
b	0.133	0.104
c	0.152	0.138
d ₁₀₀	0.089	0.083
v	0.376	0.327

* See text of paper for explanation. † Frisillo and Buljan (1972).
 ** Present study. †† Cameron et al. (1973).
 *** Smyth (1973). ††† Ohashi (1973).
 § Smyth (1974).

1.0° (mean of *A* and *B* chains) per 100°C temperature increase, but those of the *C2/c* pyroxenes change only about 0.1° to 0.2° per 100°C.

The MTEC of the *a* cell edge ($\equiv d_{100}$) in *Pbca* orthopyroxenes is larger than those of *d*₁₀₀ in *P2*₁/*c* and *C2/c* clinopyroxenes. It is conceivable that this difference is related to the different stacking sequences of pyroxene units in orthorhombic and monoclinic pyroxenes (Papike *et al.*, 1973).

The MTEC of the unit cell volume of ferrosilite was compared to that of two other orthopyroxenes (Table 10). Frisillo and Buljan (1972) obtained X-ray data

TABLE 11. Rate of Increase of Isotropic Temperature Factors ($\times 10^{-3}$)

Atom	$\Delta B/\Delta T$	Atom	$\Delta B/\Delta T$
Fe1	1.83	01A	1.73
Fe2	2.64	01B	1.80
		02A	2.14
SiA	1.21	02B	2.12
SiB	1.29	03A	2.26
		03B	2.70

* Assuming linear expansion rates.

from a powder of composition Mg_{0.8}Fe_{0.2}SiO₃. Smyth (1973) studied a single crystal having the composition Ca_{0.015}Mg_{0.305}Fe_{0.68}SiO₃. There is an inverse correlation between Fe/Mg ratio and MTEC of the unit cell volume for the three orthopyroxenes. The most Fe-rich orthopyroxene has the smallest MTEC and the most Mg-rich orthopyroxene has the largest MTEC coefficient. Similar observations have been reported for other minerals (Cameron *et al.*, 1973).

Equivalent isotropic temperature factors

The rate of increase of the equivalent isotropic temperature factors (Table 11) of both cations and anions is shown in Figure 8. The rates of increase for the four-coordinated Si atoms are significantly lower than those for the six-coordinated Fe1 and Fe2. The temperature factor for Fe2, initially larger than that for Fe1, also increases with increasing temperature at a significantly higher rate. Cameron *et al.* (1973) showed that the rate of increase of isotropic temperature factors of cations is proportional to coordination number and average *M-O* distances, and inversely proportional to charge on the cation and to electronegativity. Because both *M* sites in

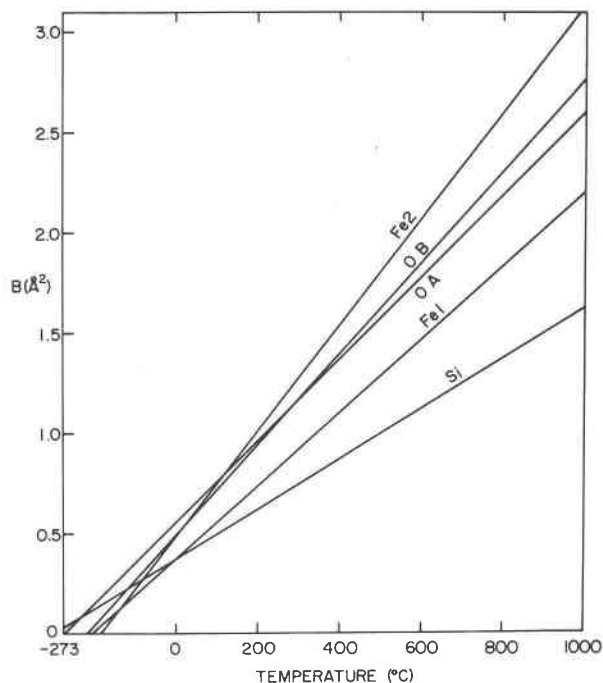


FIG. 8. Variation with increasing temperature of the equivalent isotropic temperature factors of cations and anions in orthoferrosilite. Values for oxygens of the *A* and *B* chains were averaged. The data points have been omitted to avoid overlap.

orthoferrosilite contain Fe^{2+} and because both are nominally six-coordinated, factors in addition to those listed above must be considered. The $\text{Fe}2$ polyhedron is considerably more distorted than the $\text{Fe}1$ polyhedron, and this distortion undoubtedly affects the rate of increased thermal vibration.

The rates of increase of the isotropic temperature factors of the oxygen atoms lie between those of $\text{Fe}1$ and $\text{Fe}2$. The relative rates determined for orthoferrosilite ($\text{O}3 > \text{O}2 > \text{O}1$) differ from those of the $C2/c$ pyroxenes ($\text{O}2 > \text{O}3 > \text{O}1$). The high rates of increase for the $\text{O}3$ atoms in the orthoferrosilite structure reflect their behaving as pivotal points during straightening of the tetrahedral chains. Furthermore, the rates of increase of the oxygens comprising the B chain, with one exception, are higher than those of the oxygens belonging to the A chain. This observation is probably related to the fact that the amount of straightening of the B chain is significantly greater than that of the A chain. Rates of increase of the isotropic temperature factors of Si atoms in the A and B chains and Fe^{2+} cations occupying $M1$ and $M2$ are greater than those in the $C2/c$ clinopyroxene structure (Cameron *et al.*, 1973).

Thermal ellipsoids

All atoms in the orthoferrosilite structure are located on the general positions and thus their associate thermal ellipsoids are not constrained either in orientation or shape. The ellipsoids of vibration of the $\text{Fe}1$ and $\text{Fe}2$ atoms (Table 8; Fig. 9) are both triaxial, that for $\text{Fe}2$ being larger. With increasing temperature, the rates of increase are similar for all axes with axes 2 and 3 of each ellipsoid increasing at slightly higher rates (Fig. 9). The short axes of both ellipsoids are oriented approximately parallel to the bonds involving apical oxygens, $\text{O}2A$ and $\text{O}2B$ of $\text{Fe}2$ and $\text{O}1A'$ and $\text{O}1B'$ of $\text{Fe}1$.

The ellipsoids for the two Si atoms and the six oxygen atoms are also triaxial, and their orientation varies with increasing temperature. In general, the long axes of the ellipsoids of the bridging $\text{O}3$ oxygens lie at large angles to the Si-O-Si planes.

The possibility of a displacive transition in the orthopyroxene structure

Ohashi and Finger (1973) discussed the possibility that a high-low phase transition could occur in the orthopyroxene structure. Because orthopyroxene is in many ways similar to $P2_1/c$ clinopyroxene, one could infer that transformation to a "high" structure is possible at high temperature as was observed in

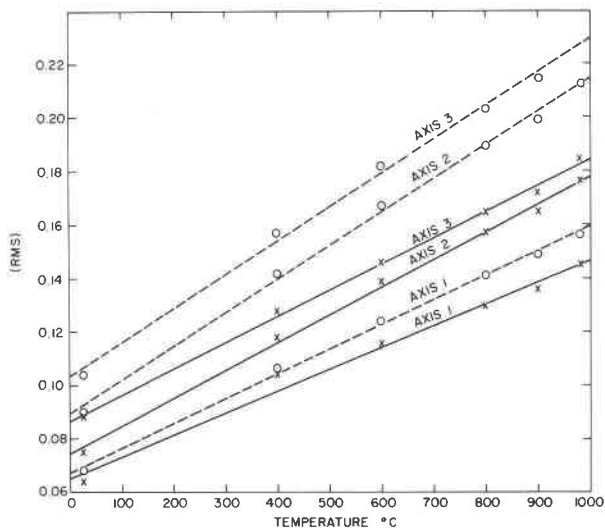


FIG. 9. Variation with increasing temperature of the magnitude of the three principal axes of the thermal ellipsoids of the $\text{Fe}2$ cation (open circles) and the $\text{Fe}1$ cation (crosses).

clinopyroxene ($P-C$ transition; Smyth, 1969; Prewitt, Brown, and Papike, 1971; Smyth and Burnham, 1972; Brown *et al.*, 1972). However, Ohashi and Finger found no evidence for such a transformation and concluded only that the space group of the "high" orthopyroxene would be $Pbca$ as in the "low" orthopyroxene with "regional" symmetry imposing non-space-group extinction conditions for reflections. The two distinct silicate chains present in the "low" orthopyroxene structure would be equivalent by the symmetry operation of "regional" 2-fold axes which arise after the hypothetical transition to the high structure.

Although the present study indicates that at a temperature near 1050°C the $\text{O}3\text{-O}3\text{-O}3$ angles of the A and B silicate chains (Fig. 7) and the volumes of the A and B tetrahedra (Tables 4 and 9) will be very similar, variations of individual Fe-O bond lengths with increasing temperature show that even the regional symmetry does not exist at high temperature. As shown in Figure 6, two sets of bonds, $\text{Fe}1$ to $\text{O}1B'$ and $\text{O}1A'$ and $\text{Fe}1$ to $\text{O}2A$ and $\text{O}1B$, became almost equivalent at high temperature but another set, $\text{Fe}1\text{-O}1A$ and $\text{Fe}1\text{-O}1B$, diverge with increasing temperature. The divergence of the latter bond lengths violates the regional 2-fold axes in the hypothetical "high" orthopyroxene structure, and suggests that orthoferrosilite would not have this high-low transition even if the $\text{O}3\text{-O}3\text{-O}3$ angles became equivalent.

Smyth (1974b) suggests another possibility for a phase transition in orthopyroxene. In a study of an

orthopyroxene crystal from lunar rock 76535, he noticed weak X-ray reflections which violated the b glide in space group $Pbca$. His conclusion was that the true space group of this pyroxene is $P2_1ca$ and that this resulted from the ordering of cations into twice as many crystallographically different octahedral sites as in the $Pbca$ structure. The occurrence of this space group was predicted by Thompson (1970) in his study of close-packed ideal models. Smyth called these two possible structures low and high orthopyroxene and proposed that there would be a phase transformation between them. In order to test whether the orthoferrosilite crystal used here might also have the $P2_1ca$ space group, we refined the structure again using the 24°C data and a structure containing one set of atoms with the refined coordinates from Table 3 and one set related to the first set through an inversion center at $1/2\ 1/2\ 1/2$. In the first few cycles of refinement the coordinates of set one were fixed and those of set two were allowed to vary. In subsequent cycles all coordinates were varied except for those of Fe1 in set one. The resulting model showed decreases in the weighted and unweighted R 's to 0.037 and 0.055, respectively. Although Hamilton's (1965) R -factor test indicates that this is a significant decrease in R , the temperature factors of twelve of the twenty atoms in the model refined to non-positive-definite values, and twenty correlation coefficients had magnitudes greater than 0.90. Furthermore, the refinement did not appear to be converging properly and the interatomic distances became unrealistic, with, e.g., Si-O distances greater than 1.80Å or less than 1.57Å.

From the experience related above, we conclude that it is not possible for us to either prove or disprove the existence of the space group $P2_1ca$ within the scope of this investigation, even though our extensive effort to refine the structure in this space group using the normal criteria for acceptable results was unsuccessful. Perhaps further, more detailed work would provide a different answer.

Conclusions

1. The mean thermal expansion coefficients (MTEC) of the cell parameters of ferrosilite decrease in the order $\alpha_c > \alpha_a > \alpha_b$. The order for $C2/c$ pyroxenes is $\alpha_b > \alpha_{d100} > \alpha_c$ and for $P2_1/c$ pyroxenes, $\alpha_c > \alpha_b > \alpha_{d100}$.
2. A linear correlation exists between the MTEC of unit cell volume and Fe/Mg ratio in three orthopyroxenes of different compositions.
3. With increasing temperature, the mean Si-O bonds and tetrahedral volumes of both SiA and SiB tetrahedra decrease slightly. The observed decrease is larger for the larger SiB tetrahedron.
4. The Fe1 and Fe2 polyhedra both expand significantly with increasing temperature. The MTEC of the mean Fe1-O distance is smaller than that of the mean Fe2-O distance, but both are significantly larger than that for Fe²⁺-O bonds in the $C2/c$ pyroxenes.
5. A new notation describing the direction of rotation (N or P) of tetrahedral chains, and the orientation between the tetrahedra and the $M2$ octahedron is introduced.
6. A and B tetrahedral chains in orthoferrosilite show a much larger magnitude of stretching than those of the $C2/c$ pyroxenes. The rate of increase of the stretching is larger at higher temperature for both chains.
7. With increasing temperature, the rates of increase of equivalent isotropic temperature factors for Si atoms are significantly lower than those for six-coordinated Fe²⁺ atoms in the $M1$ and $M2$ sites. The temperature factor for Fe²⁺ in the $M2$ site is larger than that of Fe²⁺ in the $M1$ site, and it increases at a significantly higher rate with increasing temperature.
8. Ohashi and Finger's (1973) hypothetical "high orthopyroxene" cannot form in orthoferrosilite even if the O3-O3-O3 angles of both A and B chains become equivalent at high temperature.
9. Although refinement in space group $P2_1ca$ was unsuccessful, the possibility that this space group exists for certain orthopyroxenes has not been ruled out.

Acknowledgments

This research was supported by National Science Foundation Grant No. AO-41137. D. H. Lindsley is gratefully acknowledged for synthesizing the orthoferrosilite crystals used in this study.

References

- BROWN, G. E., C. T. PREWITT, J. J. PAPIKE, AND S. SUENO (1972) A comparison of the structures of low and high pigeonite. *J. Geophys. Res.* **77**, 5778-5789.
- , S. SUENO, AND C. T. PREWITT (1973) A new single-crystal heater for the precession camera and four-circle diffractometer. *Am. Mineral.* **58**, 698-704.
- BURNHAM, C. W. (1966) Ferrosilite. *Carnegie Inst. Wash. Year Book*, **65**, 285-290.
- CAMERON, M., S. SUENO, C. T. PREWITT, AND J. J. PAPIKE (1973) High-temperature crystal chemistry of acmite, diopside, hedenbergite, jadeite, spodumene, and ureyite. *Am. Mineral.* **58**, 594-618.
- DOYLE, P. A., AND P. A. TURNER (1968) Relativistic Hartree-Fock

- X-ray and electron scattering factors. *Acta Crystallogr.* **A24**, 390–397.
- FRISILLO, A. L., AND S. T. BULJAN (1972) Linear expansion coefficients of orthopyroxene to 1000°C. *J. Geophys. Res.* **77**, 7115–7117.
- HAMILTON, WALTER C. (1965) Significance tests on the crystallographic *R* factor. *Acta Crystallogr.* **18**, 502–510.
- LINDSLEY, D. H. (1965) Ferrosilite. *Carnegie Inst. Wash. Year Book*, **64**, 148–149.
- , I. D. MACGREGOR, AND B. T. C. DAVIS (1964) Synthesis and stability of ferrosilite. *Carnegie Inst. Wash. Year Book*, **63**, 174–176.
- OHASHI, Y. (1973) *High-Temperature Structural Crystallography of Synthetic Clinopyroxene (Ca,Fe)SiO₃*. Ph. D. Thesis, Harvard University.
- , AND L. W. FINGER (1973) A possible high-low transition in orthopyroxene and orthoamphiboles. *Carnegie Inst. Wash. Year Book*, **72**, 544–547.
- PAPIKE, J. J., C. T. PREWITT, S. SUENO, AND M. CAMERON (1973) Pyroxenes: comparisons of real and ideal structural topologies. *Z. Kristallogr.* **138**, 254–273.
- PREWITT, C. T., AND A. W. SLEIGHT (1968) Structure of Gd₂S₈. *Inorg. Chem.* **7**, 1090–1093.
- , G. E. BROWN, AND J. J. PAPIKE (1971) Apollo 12 clinopyroxenes: High-temperature X-ray diffraction studies. *Proc. 2nd Lunar Sci. Conf.* **1**, 59–68.
- SMYTH, J. R. (1969) Orthopyroxene-high-low clinopyroxene inversions. *Earth Planet. Sci. Lett.* **6**, 406–407.
- (1973) An orthopyroxene structure up to 850°C. *Am. Mineral.* **58**, 636–648.
- (1974a) The high-temperature crystal-chemistry of clinohypersthene. *Am. Mineral.* **59**, 1069–1082.
- (1974b) Low orthopyroxene from a lunar deep crustal rock: a new pyroxene polymorph of space group *P2₁ca*. *Geophys. Res. Lett.* **1**, 27–29.
- , AND C. W. BURNHAM (1972) The crystal structures of high and low clinohypersthene. *Earth Planet Sci. Lett.* **14**, 183–189.
- THOMPSON, J. B., JR. (1970) Geometrical possibilities for amphibole structures: model biopyriboles. *Am. Mineral.* **55**, 292–293.

Manuscript received, March 14, 1975; accepted for publication, October 3, 1975.